ADVANCE IN MAGNETORESISTANCE MAGNETOMETER PERFORMANCES APPLIED IN EDDY CURRENT SENSOR ARRAYS.

L.Perez[1], C.Dolabdjian[1], W.Waché[2], L.Butin[2]
[1] GREYC UMR 6072 - ENSICAEN and University of Caen Basse-Normandie
[2] CEGELEC, CNDT, Brétigny S/Orge Cedex France

Abstract: The sensitivity of the magnetic sensor is important for many electromagnetic Non Destructive Evaluation (NDE) applications. Nevertheless, for successful defect detection, properties such as high linearity, large dynamic range and good spatial resolution are required. One solution comes in good using improved solid-state magnetic sensors based on Giant MagnetoResistance (GMR). In this way, we have implemented and improved elementary GMR magnetometer in order to develop NDE Eddy Current System (ECS) sensor arrays [1]. Elementary sensor operates in unshielded environment with very good performances, like high bandwidth ($f > 100$ kHz), very high slew-rate (> 30 T/s), high intrinsic dynamic (> 140 dB/√Hz at 100 Hz) and low total harmonic distortion (< 0.03 %). We compare their performances to some magnetic field sensors implemented in NDE System, focusing on the state of the art of high sensitivity magnetometer experimental investigation. The improved GMR magnetometer replaces here the detection coil used in conventional ECS, which is surrounding by an excitation setup using a classical coil.

Besides the determination of its experimental performances in alternating current techniques or remanent field measurement, we present the implementation of improved GMR magnetometer dedicated to the measurement of deep lying cracks in conducting material like aluminum and ferromagnetic plates.

Introduction: Classically, ElectroMagnetic NonDestructive Evaluation is based on probing local anomalies in the magnetic of the object under test or electromagnetic stray field of the object under test. This probing allows one to detect cracks, corrosion, inclusions or other materials defects, since the material properties in the void differ from those of unflawed material base materials.

We can distinguish three measurement categories according to the type of excitation: remanent field measurement, direct current (DC) (magnetic flux leakage) or alternating current (AC) (eddy current testing). All of these NDE techniques need an effective, inexpensive way of detecting deeply buried or small cracks in metallic parts and structures.

More, the detection of deep lying cracks, in conducting samples using eddy current testing, can be performed with magnetic sensors having high field sensitivity at low excitation frequencies, high field dynamic, high linearity, high spatial resolution, high reproducibility, low intrinsic magnetic noise, ruggedness, low inter-channel matching and large integration potentials. In order to appreciate the needed performances, it necessary to put into perspective the relative amplitudes of NDE signals, the required spatial resolution and environmental magnetic noise. Indeed, it will be shown that the requirements for noise cancellation dictate these main specifications [2] both shielded and unshielded environments. The figure 1 gives a view of the problematic of detection.

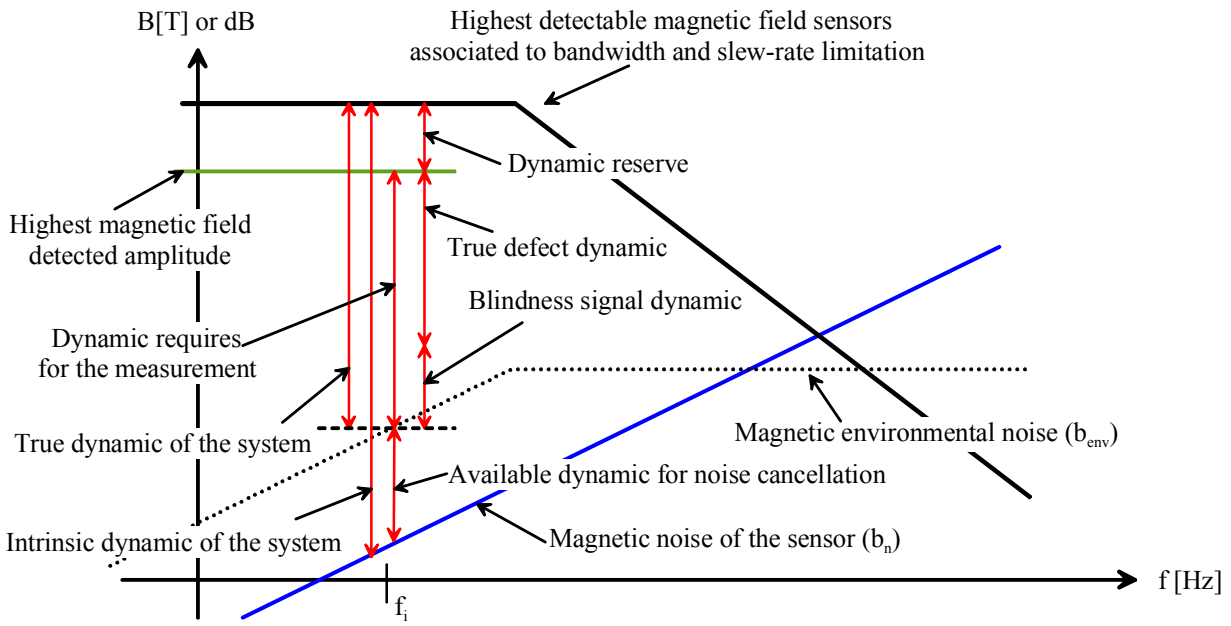

Figure 1: General problematic view of magnetic detection in NDE system, where f_s and B is, respectively, the frequency and magnetic amplitude of the detected signal.

The paper is organized as follows. The main characteristics of the improved GMR magnetometer are presented in first part and also compare to other low noise magnetic field sensors. Second part is dedicated to the ECS description, expected performances and experimental investigation of defects detection, followed by a general conclusion.

Results: We have implemented and improved the performances of Giant MagnetoResistive AA002 sensor from NVE [3] in order to develop NDE AC or DC systems. The GMR effect was associated to a field dependent ferro-antiferro magnetic coupling of ultra-thin magnetic layers through conducting layers, together with transport properties depending on the direction of the spin of free electrons with respect to the local magnetization vector [4]. The whole chip is very small (1.2 mm × 0.3 mm) and the GMR resistors occupy less than 10 % of the chip area as presented in figure 2. The classical Wheatstone bridge voltage transfer ($V_{out} = V_3 - V_4$) versus applied magnetic field is, also, presented in figure 2. The upper part of the transfer sensor nonlinearity (B > 0 T) can be fitted by a 4rd order polynomial equation. So, when we neglect the hysteresis phenomena, the output Wheatstone bridge voltage is given by: $V_{out} = k_0 + k_1 V_{dc} B_x(t) + k_2 V_{dc} B_x(t)^2 + k_3 V_{dc} B_x(t)^3 + k_4 V_{dc} B_x(t)^4$ with (0,1 mT < Bx(t) < 1 mT), where V_{dc} is the voltage Wheatstone bridge.

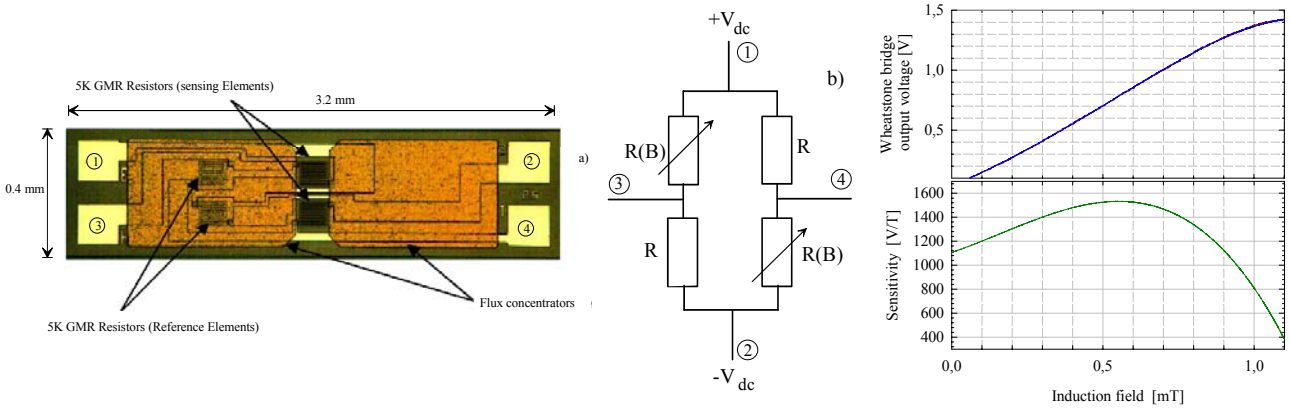

Figure 2: Photomicrograph of a NVE sensor element a), presentation of its equivalent Wheatstone bridge schematic b) and c) example of output Wheatstone bridge GMR AA002 sensor voltage response and sensitivity variations versus induction field applied in the direction of its sensing axis (output voltage measurement have been fitted with previous equation using $k_1 = 92$, $k_2 = 36\ 10^3$, $k_3 = 29\ 10^6$, $k_3 = 46\ 10^9$).

The highest voltage versus magnetic field transfer of GMR AA002 is around 100 $(V/V_{dc})/T$. We obtain maximal transfer values of around 1100-1700 V/T with ± 12 V_{dc}. This highest transfer could be achieved by using magnetic bias with small magnet or external dc field applied. Nevertheless, these sensors exhibit poor linearity, high sensitivity variation as simple magnetometer. Furthermore, it's difficult in this configuration to realize sensor arrays with high dynamics, low noise and well-known transfer.

However, it's possible to improve, notably, the linearity and dynamic of this sensor by using an improved magnetic feedback loop as resumed in figure 3. The new GMR magnetometer performances are summarized in table I and compared to classical SQUID system [5] and Fluxgate [6] truly implemented and tested in an eddy current system.

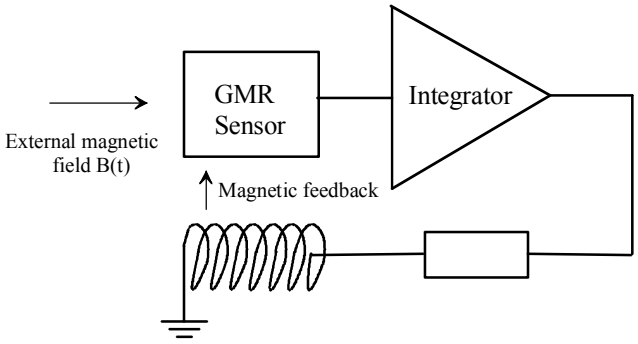

Figure 3: Sketch view of the simplified magnetic feedback loop system using GMR A002 used in the improved GMR magnetometer.

The main performances of these sensors are very comparable. Nevertheless, the high slew-rate of improved GMR magnetometer is more suitable of high magnetic disturbance rejection, which appears in industrial environment. Moreover, its intrinsic noise performance is less deteriorated in these using conditions. So, all the intrinsic dynamic of the sensors will be fully used for defect detection. Furthermore, multi sensor system development is also possible and very simpler to implement in this case. Each sensor didn't need individual usual external magnet bias as needed to these sensors.

In the first measurement, we have used a single improved GMR magnetometer. The excitation setup uses a classical coil surrounding the GMR magnetometer (Inducer), as presented in figure 4. It uses to provide depth selective information about the defect. The coil size is changeable. The length of the GMR sensor limits its inner diameter "d" to around 4 mm. The orthogonal configuration excitation-sensitive axis permits to achieve a reduction of the excitation field at the magnetometer of up to 40-60 dB, compared to the field at the sample under test.

	Improved GMR magnetometer	SQUID [5]	Fluxgate [6]
Supply voltage	± 12 V	± 12 V	± 12 V
First stage gain output sensitivity	≈ 1600 V/T	≈ 1,000 - 3000 V/T	≈ 100,000 V/T
Bandwidth	dc to > 300 kHz	dc to ≈ 1 MHz	dc to 3 kHz
Slew-rate	Theoretical > 160 V/T Measured >37.5 T/s*	≈ 0.1 to 1 mT/s	

Distortion (Total Harmonic Distortion) F = 10 Hz - 1 kHz	Amplitude: ± 1mT$_{peak}$ < 0.03 %* Theoretical : < 0.001%		Amplitude: ? ≈ 0.0015%
Noise density	5/√f nT/ √Hz f< 1 kHz ≈ 150 pT/ √Hz f > 1 kHz	≈ pT/√Hz f > 1 Hz	≈ 2.5 pT/√Hz f > 1 Hz
Dynamic F = 10 Hz - 100 Hz - 1 kHz	127 - 137 dB/√Hz - 147 dB/√Hz	≈ 140 dB/√Hz - 120dB/ √Hz	≈ 150 dB/√Hz - 140 dB/√Hz
Full Scale field range	± 4.5 mT	± few µT	± 120 µT
dc field offset temperature drift			0.1 -0.6 nT/°C
Spatial resolution	> 1 mm** Limited by the encapsulation		> 15 mm Limited by the encapsulation
Hysteresis	Negligible	Negligible	
Perpendicular field sensitivity	Cos(β)**	Cos(β)**	Cos(β)**
Operating temperature range	-40°C to + 85°C*	-119°C	-40°C to 70°C
Insensitivity to magnetic shock	> 10 mT		
Encapsulated sensor external size	0.7 mm × 0.7 mm × 4 mm	1cm × 1 cm	1 cm × 0.6 mm
Cryogenic limitation Size &	No	Yes	No

* Results limited by the measurement system dynamic and linearity
** Datasheet or Measured

Table 1: Comparison of the improved GMR magnetometer performances to SQUID and fluxgate magnetometer examples.

It improves, in this way, the dynamic range defect detection by more than three orders of magnitude compared to classical systems. If we include, too, the difference of classical system and improved GMR magnetometer intrinsic dynamic, the actual improved dynamic is, in that case, more than 60 dB to 100 dB to classical systems in the 10 to 10 kHz range of frequencies.

A sinusoidal current source (Generator) provides a current through the induction coil I_c of controlled amplitude (up to 20 mA to 1 A) and frequency (f_0) between (1 Hz and 100 kHz). A high dynamic lock-in amplifier generates the in-phase and out-phase voltage component corresponding to field image amplitude detected by the GMR magnetometer. Theses demodulated responses were low pass filtered, detected by 6½ digits multimeters and recorded with PC. The sample rate of the recorded data could be adapted to the scanning velocity to 0.33 - 100 samples/s. Thus, the full-scale or instrinsic dynamic of the magnetometer can be more than:

$$\left(\frac{\text{full scale field range}}{2} \frac{\sqrt{f_0}}{5\,10^{-9}} \right)_{dB} = 117 \text{ dB} + 20 \text{ Log}(\sqrt{f_0}) \text{ dB}/\sqrt{\text{Hz}}$$

with $0.01 < f_0 < 1$kHz in 1 Hz post-detection filtering to a maximal value of around 150 dB/√Hz.

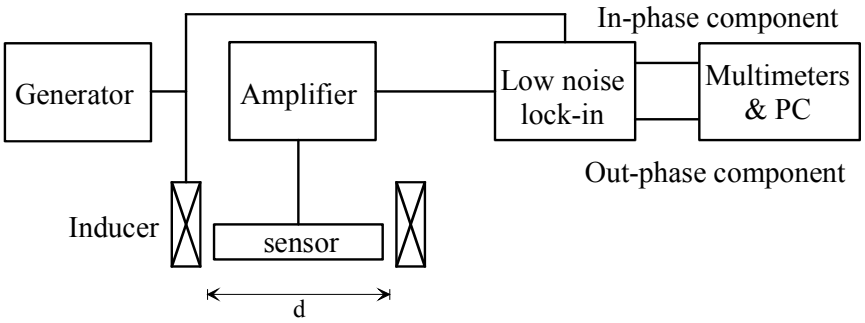

Figure 4: Schematic diagram of the measurement configuration.

Discussion: An experimental benchmark was developed to assess the feasibility of the improved GMR CND sensor. Various calibrated defects were machined into the subsurface of an aluminum plate (16cm*5cm*1cm) or on a similar ferromagnetic plate. The dimensions of the subsurface defects are given in table II and shown in figure 6. The distance between each transverse long crack is 40 mm. The minimal sensor lift-off could be around 0 to 200 µm. The noise level of the sensors was, here, deteriorated by the environmental noise induced in the laboratory, by experimental benchmark, as shown in figure 8. The improved GMR magnetometer magnetic noise was increased by a factor of 10 to the noise sensor reference.

The field to voltage transfer of the ECS is, in Alternating Current measurement benchmark of 51 kV/T. Thus, the true dynamic of the ECS AC measurement is 93 dB in 1 hertz bandwidth (for f_0 = 100 Hz) and in the laboratory environmental condition as presented in figure 5.

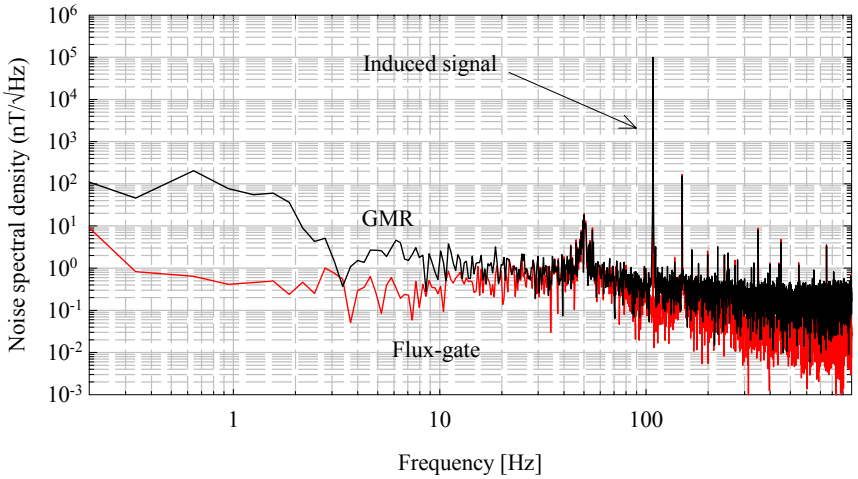

Figure 5: Environmental noise spectral density b_{env} measures with improved GMR magnetometer and compare to flux-gate reference magnetometer measurements.

This performance could be improved to 133 dB by reducing, first, one stage gain of 20 dB and second, the environmental noise to the sensor noise level by gradiometric structure using. Similarly, the field to voltage transfer of the ECS, remanent magnetic field measurement, is 1.6 kV/T and the true dynamic is more than 120 dB/√Hz.

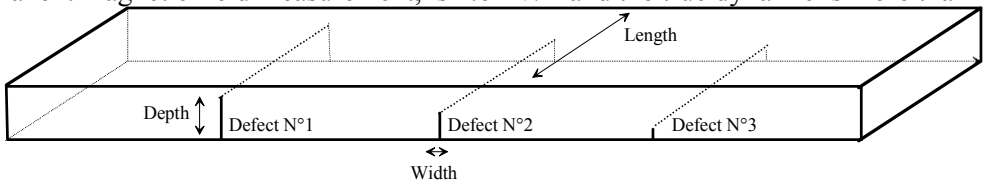

a) Scheck-view of experimental plate (aluminum or ferromagnetic)

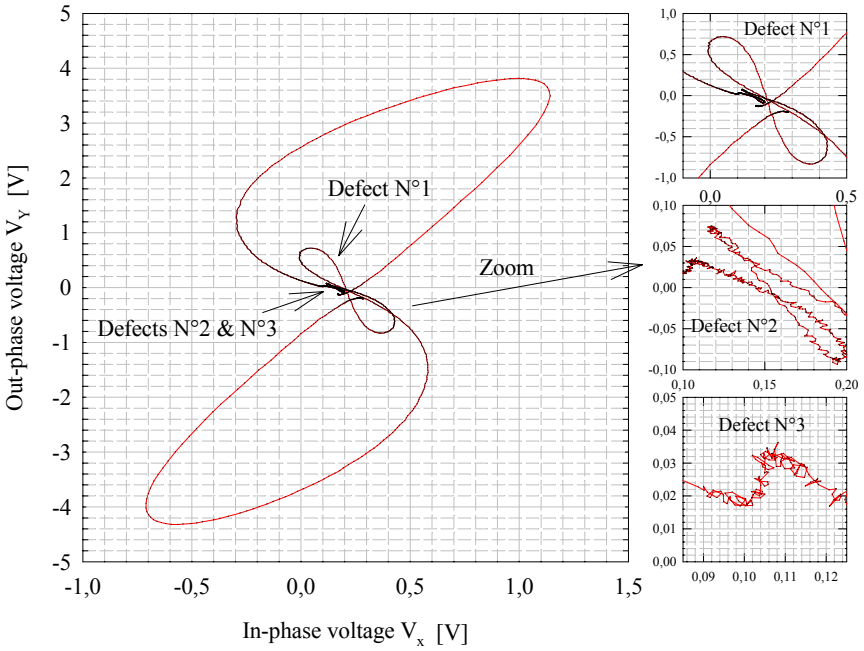

a) aluminum plate under test - (alternating current measurement)

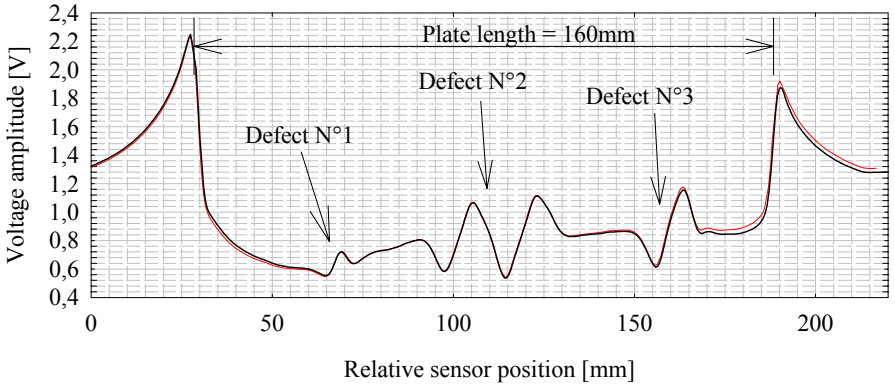

b) ferromagnetic plate under test - (remanent magnetic field measurement)

Figure 6: Sketch view of the sample under test a), output Lissajous curve obtain with previous condition b) (voltage to magnetic field transfer = 51 kV/T) - (Coil diameter ≈ 0.5 cm, Number of turns = 500) - (f_0 = 100 Hz, I_c = 37 $mA_{crête}$) - (speed of detection = 5 mm/s) - (last pass filter cut off frequency = dc -10 Hz), output remanent magnetic field measured under ferromagnetic plate c) (voltage to magnetic field transfer = 1.6 kV/T) (speed of detection = 25 mm/s) - (last pass filter cut off frequency = dc -10 Hz).

The speed detection υ is only limited, in this ECS, by the last first order low past-filtering time constant t_i and the spatial length d of field response. Here, d could be considered equivalent to the excitation coil diameter. So, if we want to observe 90% of the expected pulse response amplitude, the speed detection can be lower than $d/(3\ t_i)$, as given in table 2. We have, also, summarized in tables 3, 4, 5 some element of feasibility and comparison of detection of three different kinds of magnetometer (improved GMR ECS, SQUID [7] and fluxgate [6]). The dynamic range defect detection of EDC AC and remanent magnetic field measurement is, respectively, defined by:

$$D_{DRDD} \approx 20\ \mathrm{Log}\left(\frac{B_{mes}\ nb\cdot I_C}{\sqrt{b_n^2 + b_{env}^2}}\right)\ \mathrm{dB}\ \text{and}\ D_{DRDD} \approx 20\ \mathrm{Log}\left(\frac{B_{mes}}{\sqrt{b_n^2 + b_{env}^2}}\right)\ \mathrm{dB},$$

where B_{mes} is the peak to peak magnetic amplitude divided by the excitation amplitude current I_C per turns and $\overline{b_n^2}$, $\overline{b_{env}^2}$ is, respectively, the output equivalent magnetic noise induce by the sensor and the environment in the system bandwidth.

Subsurface defect	Length [mm]	Width [µm]	Depth [mm]	B* [nT]	SNR [dB]	Best expected value of SNR [dB]	Speed [mm/s]
Defect N°1	50	500	8	5200	47	67	5 mm/s
Defect N°2	50	500	5	284	21	41	5 mm/s
Defect N°3	50	500	2	83	9	29	5 mm/s

*limited by d/(3 t_i). d is around 0.5 cm

Table 2-a: Geometry of defects into the subsurface **10 mm aluminum plate** and performances of the ECS AC measurement, using the improved GMR magnetometer, as shown in figure 6.

Subsurface defect	Length [mm]	Width [µm]	Depth [mm]	B* [mT]	SNR [dB]	Best expected value of SNR [dB]	Speed [mm/s]
Defect N°1	50	500	8	125	87	107	25 mm/s
Defect N°2	50	500	5	375	96	116	25 mm/s
Defect N°3	50	500	2	350	95	115	25 mm/s

*limited by d/(3 t_i). d is around 0.5 cm

Table 2-b: Geometry of defects into the subsurface **10 mm ferromagnetic plate** and performances of the ECS remanent magnetic field measurement, using the improved GMR magnetometer, as shown in figure 6.

Subsurface defect	Length [mm]	Width [µm]	Depth [mm]	B [nT/(nb·A)]	SNR [dB]	Best expected value of SNR [dB]	Maximal Speed [mm/s]*
Defect N°1	50	500	8	280	32 + 20 Log(nb·I_c/√f_i)	52 + 20 Log(nb·I_c/√f_i)	d/(3 t_i)
Defect N°2	50	500	5	14.25	6 + 20 Log(nb·I_c/√f_i)	26 + 20 Log(nb·I_c/√f_i)	d/(3 t_i)
Defect N°3	50	500	2	4.45	-7 + 20 Log(nb·I_c/√f_i)	13 + 20 Log(nb·I_c/√f_i)	d/(3 t_i).

Table 2-c: Geometry of defects into the subsurface **10 mm aluminum plate** and expected performances of the ECS AC measurement using the improved GMR magnetometer versus I_C, which are the current amplitude of the excitation frequency and $f_i = 2\pi/t_i$.

Subsurface defect	Length [mm]	Width [µm]	Depth [mm]	B [nT/(nb·A)]	Best expected value of SNR [dB] in 1 Hz Bandwidth	Experimental SNR [dB]*	f_0 [Hz]
[7]	60	2000	1.5	2	58 + 20 Log(nb·I_c/√f_i)	30	100

* noise environment of around 100 pT/√Hz reduce to 10 pT/√Hz by gradiometric measurement

Table 3: Geometry of flaws machined into the subsurface **6 mm aluminum plate** and relative performances of the detection of SQUID gradiometer example in ECS AC measurement.

Subsurface defect	Length [mm]	Width [µm]	Depth [mm]	B [nT/(nb·A)]	Best expected value of SNR [dB] in 1 Hz Bandwidth	Experimental SNR [dB]	f_0 [Hz]
[6]	40	600	3	0.4	$44 + 20\ \mathrm{Log}(nb \cdot I_c/\sqrt{f_i})$	?	180

Table 4: Geometry of flaws machined into the subsurface **13 mm aluminum plate** and best performances of the detection of fluxgate magnetometer example in ECS AC measurement.

Conclusions: Solid state magnetic field sensors, like GMR, have an important potential to modernize measurement and control in areas which the magnetic fields, produced either by bias magnets or electric current, have been above its intrinsic magnetic noise around earth'field. Nevertheless, these sensors have intrinsic poor linearity, low dynamic and reproducibility. Their use, in feedback loop configuration, improves notably their performances, as we present. The performance of the improved GMR magnetometer ECS are very comparable to the state of the art, in term of dynamic, of ECS system using SQUID or Flux-gate, if we can control the current amplitude in the inducer or the amplitude of the magnetic noise environment. More, these improved GMR sensors have a potential for large integration and high slew rate, which are required for NDE or NDI system development. Future investigation is made to measure the spatial resolution of the system versus defect detection.

Acknowledgement: This work was, partly, supported by European Regional Development Fund (FEDER) and French National Territories Development Fund (FNADT).

References:

[1] L. Butin, G. Waché, L. Perez, C. Dolabdjian, "New NDE perspectives with Magnetoresistance array technologies. From research to industrial applications", 6th World Conference on Non-Destructive Testing in Montréal, 2004

[2] J. Vrba, J. McKay, "Character and acquisition of multi channel biomagnetic Data", ISEC'97, 105-108(1997)

[3] NVE Corporation, 11409 Valley View RoadEden Prairie, MN 55344-3617, http://www.nve.com/

[4] S. Tumanski, Institute of Physics, Series in Sensors, "Thin Film Magnetoresistive Sensors"

[5] M.v. Kreutzbruck, K. Allweins, G. Gierelt, H.J. Krause, S. Gärtner, W. Wolf, "Defect detection in thick aircraft samples using HTS SQUID magnetometers", Physica C 368, 85-90(2002)

[6] M.v. Kreutzbruck, K. Allweins, C. Heiden, "Fluxgate-magnetometer for the detection of deep lying defects", 5th World Conference on Non-Destructive Testing Roma, 15-21 October, 2000

[7] J.T. Jeng, H.E. Horng, H.C. Yang, "High TC SQUID magnetometers and gradiometers for NDE application", Physica C 368, 105-108(2002)